Quantification of relative contribution of Antarctic ozone depletion to increased austral extratropical...

Article *in* Journal of Geophysical Research Atmospheres · February 2016

DOI: 10.1002/2015JD024247

CITATIONS
2

READS
66

3 authors, including:

Kaixu Bai
East China Normal University
15 PUBLICATIONS **30** CITATIONS
SEE PROFILE

Ni-Bin Chang
University of Central Florida
329 PUBLICATIONS **6,223** CITATIONS
SEE PROFILE

AGU PUBLICATIONS

JGR

Journal of Geophysical Research: Atmospheres

RESEARCH ARTICLE
10.1002/2015JD024247

Key Points:
- Linkages between austral extratropical precipitation and Antarctic ozone are phenomenal
- The Antarctic ozone depletion drives austral extratropical precipitation pattern
- The equatorial Pacific SST can modulate the austral precipitation variability

Correspondence to:
N.-B. Chang,
nchang@ucf.edu

Citation:
Bai, K., N.-B. Chang, and W. Gao (2016), Quantification of relative contribution of Antarctic ozone depletion to increased austral extratropical precipitation during 1979–2013, *J. Geophys. Res. Atmos.*, *121*, doi:10.1002/2015JD024247.

Received 19 SEP 2015
Accepted 17 JAN 2016
Accepted article online 22 JAN 2016

Quantification of relative contribution of Antarctic ozone depletion to increased austral extratropical precipitation during 1979–2013

Kaixu Bai[1,2], Ni-Bin Chang[2], and Wei Gao[1,3]

[1]Key Laboratory of Geographic Information Science, Ministry of Education, East China Normal University, Shanghai, China, [2]Department of Civil, Environmental, and Construction Engineering, University of Central Florida, Orlando, Florida, USA, [3]USDA UV-B Monitoring and Research Program, Natural Resource Ecology Laboratory, and Department of Ecosystem Science and Sustainability, Colorado State University, Fort Collins, Colorado, USA

Abstract Attributing the observed climate changes to relevant forcing factors is critical to predicting future climate change scenarios. Precipitation observations in the Southern Hemisphere indicate an apparent moistening pattern over the extratropics during the time period 1979 to 2013. To investigate the predominant forcing factor in triggering such an observed wetting climate pattern, precipitation responses to four climatic forcing factors, including Antarctic ozone, water vapor, sea surface temperature (SST), and carbon dioxide, were assessed quantitatively in sequence through an inductive approach. Coupled time-space patterns between the observed austral extratropical precipitation and each climatic forcing factor were firstly diagnosed by using the maximum covariance analysis (MCA). With the derived time series from each coupled MCA modes, statistical relationships were established between extratropical precipitation variations and each climatic forcing factor by using the extreme learning machine. Based on these established statistical relationships, sensitivity tests were conducted to estimate precipitation responses to each climatic forcing factor quantitatively. Quantified differential contribution with respect to those climatic forcing factors may explain why the observed austral extratropical moistening pattern is primarily driven by the Antarctic ozone depletion, while mildly modulated by the cooling effect of equatorial Pacific SST and the increased greenhouse gases, respectively.

1. Introduction

Unlike ground-level ozone, which is considered a pollutant and causes a number of health problems, stratospheric ozone plays a critical role in protecting life forms on Earth from the Sun's harmful ultraviolet (UV) light, by absorbing high frequency UV radiation through photochemical processes, even with its small concentrations in the atmosphere. In addition to this shielding effect, stratospheric ozone plays an important role in modulating regional climatic changes, particularly in the Southern Hemisphere (SH). It is observed that the SH has undergone remarkable changes over the past decades, such as rapid warming in the western Antarctica [*Ding et al.*, 2011; *Bromwich et al.*, 2012], expanded Antarctic sea ice [*Sigmond and Fyfe*, 2014], regional rainfall decline in Australia [*Delworth et al.*, 2014], austral subtropical moistening [*Feldstein*, 2011; *Kang et al.*, 2011, 2013; *Gonzalez et al.*, 2013], and summer warming in southern Africa [*Manatsa et al.*, 2013]. Further investigations suggest that these observed climatic changes should be substantially attributed to the joint effects of anthropogenic forcing from increased greenhouse gases (GHGs) concentration in the atmosphere and dramatic ozone depletions over Antarctica.

The radiative forcing (RF) of stratospheric ozone depletion is small compared to that of well-mixed GHGs (i.e., $-0.05 \pm 0.10\,\mathrm{w\,m^{-2}}$ global annual mean RF of stratospheric ozone in comparison with $+2.6 \pm 0.3\,\mathrm{w\,m^{-2}}$ of GHGs in 2005 relative to preindustrial levels) [*Forster et al.*, 2007; *Previdi and Polvani*, 2014]. Nevertheless, a depleted Antarctic ozone layer is believed to have significant impacts on the SH climate, and its effect is not confined just to the vicinity of Antarctica but extends over much of the SH, even reaching the tropics [*Son et al.*, 2009; *Feldstein*, 2011]. Similar to the effects of increased GHGs in the atmosphere, Antarctic ozone depletion-induced stratospheric cooling alters the atmospheric circulation pattern, characterized by a poleward shift of the westerly jet and the Hadley cell boundary. The direct consequences of these shifts are significant weather and climate changes at the surface, such as a strengthening of the polar vortex, a poleward shift of storm tracks in the SH middle-to-high latitudes, and a poleward expansion of dry zones in the tropics [e.g., *Son et al.*, 2008, 2009; *Arblaster et al.*, 2011; *Feldstein*, 2011; *Kang et al.*, 2011; *Perlwitz*, 2011; *Delworth et al.*, 2014].

While most modeling results suggest that the observed climatic changes in the SH should be substantially attributed to dramatic ozone depletion over Antarctica [e.g., *Son et al*., 2010; *Kang et al*., 2011; *Shaw et al*., 2011; *Eyring et al*., 2013; *Gonzalez et al*., 2013; *Manatsa et al*., 2013; *Previdi and Polvani*, 2014], other modeling analyses present conflicting results indicating that these SH climatic changes result primarily from increasing GHGs in the atmosphere, rather than stratospheric ozone depletion [e.g., *Fyfe et al*., 2012]. Although these conflicting results could be ascribed to incorrect specification of ozone or oversimplification of chemical and dynamic interactions in modeling processes [*Waugh et al*., 2009; *Perlwitz*, 2011], it illustrates the need to find additional evidence to confirm the relative role of each climatic forcing factor.

Due to the implementation of Montreal Protocol and its amendments dedicated for phasing out the use of ozone depleting substances, signs of ozone recovery have been observed since the early 21st century, and the ozone layer is projected to return to the pre-1980 level by the middle of this century [*World Meteorological Organization* (*WMO*), 2011, 2014]. Yet simulations suggest a reverse climatic effect, indicating that the recovery of ozone layer will cancel out changes induced by increasing GHGs concentrations, which means the future climate in the SH will largely depend on the competing effects between these two climatic forcing factors, despite cancelation being only a summertime event [*Perlwitz et al*., 2008; *Hu et al*., 2011; *Perlwitz*, 2011]. Given the joint effects of increased concentration of GHGs and depleted stratospheric ozone on the SH climate, differential contributions from each forcing factor should be clearly quantified to clarify those conflicting results. Such an elevated understanding of the contributions resulting from different forcing factors in modulating current climate can certainly promote accurate prediction of future climate change scenarios. Therefore, quantifying climatic responses to each forcing factor is essential for not only the climate change detection and attribution but also the fundamental physical mechanisms to better predict changing climate in the future [*McLandress et al*., 2010].

It is known that the SH extratropics have experienced significant austral summer moistening compared to other regions over the time period of 1979 to 2013 (Figure 1a). In the view of temporal domain, the precipitation variability over those regions is highly associated with the variation of the Antarctic ozone hole size (Figure 1b). Since there is no significant moistening trend observed in seasons other than summer in this region, and a consensus that the GHGs have no seasonal forcing effects throughout the year [*Previdi and Polvani*, 2014], we may hypothesize that this observed wetting climate could be driven primarily by the dramatic ozone depletion over Antarctica. To demonstrate the predominant role of Antarctic ozone depletion in triggering this observed wetting climate, this study aims to employ inductive approaches to investigate relevant linkages between precipitation changes and four different forcing factors in time-space domain and to quantify the precipitation responses to each climatic forcing factor. In this study, four different forcing factors, including carbon dioxide, water vapor, sea surface temperature (SST), and total column ozone (TCO), were selected to represent climatic forcing from GHGs, ocean-atmosphere interactions, and atmospheric ozone variability. The key question to be answered here is to what extent the observed austral extratropical moistening can be attributed to Antarctic ozone depletion relative to other forcing factors.

2. Data

2.1. Precipitation

To investigate the austral extratropical precipitation responses to aforementioned forcing factors, gridded precipitation products generated from the Global Precipitation Climatology Project (GPCP) Version 2.2 Combined Precipitation Data Set over the time period of 1979–2013 were applied. GPCP was initially established by the World Climate Research Program and subsequently attached to the Global Energy and Water Exchange program to quantify the spatiotemporal distribution of global precipitation by blending various estimates together [*Adler et al*., 2003; *Huffman et al*., 2009]. Data from more than 6000 rain gauge stations, along with satellite geostationary, low-orbit infrared, passive microwave, and sounding observations, were merged on a 2.5° global grid to estimate monthly rainfall since 1979. To date, these combined rainfall estimates provide the most thorough analysis of rainfall at the global scale.

2.2. ERA-Interim TCO Reanalysis

ERA-Interim is the latest reanalysis (third generation reanalysis) project completed by the European Centre for Medium Range Weather Forecasts (ECMWF) to continue the previous ERA-40 reanalysis project. ERA-Interim provides a global analysis on the state of the atmosphere, land, and sea surface conditions from 1979 to the present,

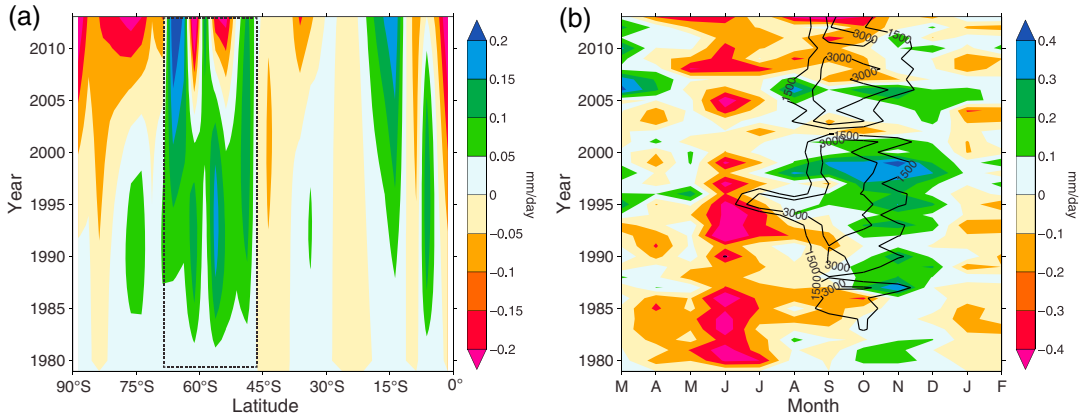

Figure 1. Precipitation changes over the time period of 1979–2013 in the Southern Hemisphere (SH). (a) Observed long-term precipitation trends in the SH. (b) Monthly zonal mean (outlined region in Figure 1a) precipitation anomalies (relative to the 1979 level) varying with Antarctic ozone hole size (thick black contour lines). Monthly Antarctic ozone hole size is represented by the number of grids with total column ozone value lower than 220 DU.

which has been continuously updated on a near real-time basis by using a data assimilation system. It describes the evolution of precipitation, soil moisture, soil temperature, and snowpack. Analyses from the ERA-Interim are gridded at different spatial resolutions, ranging from 0.125° × 0.125° to 3° × 3°, with temporal resolutions varying from hours to months. General discussions on the ERA-Interim assimilation system can be found in *Dee et al.* [2011].

Ozone analyses have been included in the ERA data assimilation system since the project of ERA-40, making it the largest data set of meteorologically consistent three-dimensional ozone fields to date. The main characteristics of ECMWF ozone assimilation system used in ERA-40 project are described in detail in *Dethof and Hólm* [2004]. As stated there, the first guess of ozone concentration was derived from an updated version of *Cariolle and Déqué* [1986] scheme. In the scheme, the evolution of ozone field was described by a tracer transport equation including a parameterization of photochemical sources and sinks. The ozone continuity equation was expressed as a linear relaxation toward a photochemical equilibrium for the local value of the ozone mixing ratio, temperature, and overhead ozone column via generation of linear photochemistry schemes and the ozone distributions. In addition, an ozone destruction term was used to parameterize the heterogeneous chemistry as a function of the equivalent chlorine content for the actual year [*Dragani*, 2011]. Most of these parameterizations are still applied in the ERA-Interim, but a number of changes and improvements to the model physics and parameterizations have been implemented. In addition, a four-dimensional variational data assimilation scheme (4-D-Var) was applied as opposed to the 3-D-Var scheme used in ERA-40, by incorporating a variational bias correction scheme (VarBC) to automatically detect and correct for satellite observation biases [*Dragani*, 2011]. Detailed discussions in regard to those changes and improvements can be found in literatures, such as *Cariolle and Teyssèdre* [2007] and *Dee and Uppala* [2009].

Ozone data have been recorded from various instruments and assimilated in ERA-Interim reanalysis. They include not only the ozone data from solar backscatter ultraviolet-type instruments on board the NIMBUS-7 and NOAA-9/11/16/17/18 satellites, TOMS on board METEOR-3, and Earth Probe platform but also new ozone data sets from the latest ozone monitoring projects, including the Global Ozone Monitoring Experiment at Europe and the Ozone Monitoring Instrument (OMI) on board NASA's Aura platform. The utilization of more accurate satellite observations has made the new ozone reanalysis more robust by benefitting from any further improvement in its accuracy. Compared to other multisensors directly merged TCO data sets, the ERA-Interim TCO reanalysis has its distinct advantage due to the fully global scale coverage. As reported by *Dragani* [2011], the ERA-Interim TCO reanalysis have an accuracy typically within ±5 Dobson unit (2.69×10^{16} molecules cm^{-2}) (DU) (about ±3%) from the ground-based reference TCO observations, with a 2% underestimation of the Ozone Monitoring Instrument (OMI) TCO observations between 50°N and 50°S. These statistics indicate fair accuracy of the ERA-Interim TCO reanalysis, which satisfies our long-term climatic change attribution needs, because the most advanced OMI has a TCO retrieval accuracy of 2% [*McPeters et al.*, 2008; *Antón et al.*, 2009].

Therefore, monthly ERA-Interim TCO reanalysis data gridded by 1.5° × 1.5° over the time period of 1979 to 2013 were applied to investigate possible linkage between austral extratropical precipitation and Antarctic

Table 1. Description of Data Sources Used in This Study

Variable	Type	Unit	Spatial Resolution	Temporal Resolution	Data Set
Precipitation	Surface	mm/day	2.5°	Monthly	GPCP V2.2
Total Column Ozone	Integrated	DU	1.5°	Monthly	ERA-Interim
Water Vapor	Integrated	kg/m^2	1.5°	Monthly	ERA-Interim
Sea Surface Temperature	Surface	K	1.5°	Monthly	ERA-Interim
Carbon Dioxide	Integrated	ppm	n/a	Monthly	ESRL/NOAA
U wind	Pressure level	m/s	1.5°	Monthly	ERA-Interim

ozone depletion. In addition to the TCO reanalysis, global scale SST and water vapor reanalysis from the ERA-Interim project were also applied to represent possible climatic forcing from SST and GHGs. Meanwhile, the ERA-Interim *U* wind (i.e. East-west wind) at varying pressure levels was also applied to investigate the linkage between Antarctic ozone depletion and atmospheric circulation changes. Detailed information on these products can be found in Table 1. Due to the lack of long-term gridded continuous monitoring of carbon dioxide at the global scale, a monthly carbon dioxide time series recorded at Mauna Loa was used as a representative to diagnose the possible forcing effects of increasing global carbon dioxide concentrations [*Thoning et al.*, 1989; *Buermann et al.*, 2007].

3. Methods

In order to quantify austral extratropical precipitation responses to each climatic forcing factor, two different methods were applied for different purposes. First, the maximum covariance analysis (MCA) was applied to detect inherent linkages between austral extratropical precipitation and each forcing factor at the spatial domain, by identifying the maximum covariance in the temporal domain. From the identified leading coupled modes, principal time series of each variable representing the primary contribution and response were extracted for further modeling processes. With these derived representative time series, a machine learning tool called extreme learning machine (ELM) was then used to establish complex interactions between these forcing factors and the austral extratropical precipitation. Once reliable relationships were established, sensitivity tests were conducted to quantify precipitation responses to each climatic forcing factor.

3.1. MCA

MCA is designed to look for patterns in two time-space data sets by maximizing the covariance between them, leading to the enhancement of understanding of their relevant interactions [*Bretherton et al.*, 1992]. The method relies on decomposing two parameters covariance matrix into different coupled modes, with each mode representing a unique time-space pattern explaining certain percentage of total covariance [*Bretherton et al.*, 1992; *Wallace et al.*, 1992]. Given two time-space data matrices $X(i) = \{x_1(i), \ldots, x_n(i)\}$ and $Y(i) = \{y_1(i), \ldots, y_m(i)\}$, $i = 1, \ldots, N$ represents joint observations of X and Y (i.e., time series):

$$X = \begin{bmatrix} x_1(1) & \cdots & x_n(1) \\ \vdots & \ddots & \vdots \\ x_1(N) & \cdots & x_n(N) \end{bmatrix} \tag{1}$$

$$Y = \begin{bmatrix} y_1(1) & \cdots & y_m(1) \\ \vdots & \ddots & \vdots \\ y_1(N) & \cdots & y_m(N) \end{bmatrix} \tag{2}$$

Thus, X and Y are two matrices having a dimension of $N \times n$ and $N \times m$, respectively, where N is the number of samples in the temporal domain while n and m represent the number of grid points or stations in the spatial domain. The cross-covariance matrix between X and Y can be calculated as

$$C_{xy} = \begin{bmatrix} \mathrm{cov}(x_1, , y_1) & \cdots & \mathrm{cov}(x_1, , y_m) \\ \vdots & \ddots & \vdots \\ \mathrm{cov}(x_n, , y_1) & \cdots & \mathrm{cov}(x_n, , y_m) \end{bmatrix} = \frac{1}{N-1} X^T Y. \tag{3}$$

As shown in equation (3), the cross-covariance matrix C_{xy} has a dimension of $n \times m$, which represents the integrated realization of possible couplings between X and Y in the time-space domain. To identify the distinctive

Table 2. Comparisons Between Different Inductive Approaches Used for Detection and Attribution in Earth Systems Analysis

	Pros	Cons	References
Canonical Correlation Analysis (CCA)	Easy to implement and maximized correlation	Data dependent, large sampling variability, knowledge-based interpretation, and less accurate	[*Tippett et al*., 2008; *Niranjan Kumar and Ouarda*, 2014]
Principle Component Analysis (PCA)	Principle features extraction, reduced dimension, contribution factors, and rotated solutions	One eigenvector, maximized variance instead of covariance, and knowledge-based interpretation;	[*Abdi and Williams*, 2010]
Maximum Covariance Analysis (MCA)	Self-adaptive, computational efficient, left and right eigenvectors acquired simultaneously, and maximized covariance	Knowledge-based interpretation and left and right patterns cannot be rotated independently	[*Wallace et al*., 1992; *Ding et al*., 2011]
Clustering	Visual plausible and easy to implement	Less accurate and data dependent	[*Steinbach et al*., 2001]
Bayesian Approach	Integrated information, incorporate independent information, Probabilistic, and less sensitive to bias	Subjective and hard to use at large scale	[*Hasselmann*, 1998]
Optimal Fingerprinting	Objective quantitative significance estimates and efficient	Less reliable, data length dependent, and prior knowledge of the signal and noise	[*Hegerl et al*., 1996; *Barnett et al*., 2005]
Association Rule	Physical meaningful and more accurate	Complicated, prior knowledge, and computation intensive	[*Dhanya and Nagesh Kumar*, 2009]

coupled patterns between X and Y, singular value decomposition (SVD) was applied to decompose the cross-covariance matrix C_{xy} into different mode:

$$C_{xy} = U^T \Sigma V, \tag{4}$$

where $U = \{u_1(n), u_2(n), \ldots, u_r(n)\}$ and $V = \{v_1(m), v_2(m), \ldots, v_r(m)\}$. r is the total number of real positive singular values $\{\sigma_1, \sigma_2, \ldots, \sigma_r\}$ in Σ, which are sorted in a descending order as $\sigma_1 \geq \sigma_2 \geq \sigma_3 \ldots \geq \sigma_r$. Therefore, the maximum covariance can be obtained from the leading SVD mode of C_{xy}, such as the first left (u_1) and right (v_1) singular vector, representing the maximized X and Y pattern, respectively. As suggested in equation (4), derived SVD modes maximize the cross covariance between X and Y, and the following patterns are spatially orthogonal to the previous modes. This advantage makes it clearer to identify the possible linkages between each climatic forcing factor and response regions in the prescribed spatial domain. Meanwhile, the time-space patterns of each mode can be realized by projecting relevant singular vectors onto the data:

$$a_j = X^T u_j \tag{5}$$

$$b_j = Y^T v_j, \tag{6}$$

where $j = 1, \ldots, r$. Since each SVD mode explains an amount σ_k^2 of the overall squared covariance in C_{xy}, the contribution of each coupled mode relative to the total covariance can be signified in terms of the squared covariance fraction (SCF) by

$$\mathrm{SCF}_k = \frac{\sigma_k^2}{\sum_k^r \sigma_k^2}. \tag{7}$$

Unlike other relevant methods to isolate coupled patterns between two time-space related parameters, such as the Canonical Correlation Analysis (CCA), which mainly characterizes the maximized correlation between pair-wised parameters and can be severely affected by random sampling fluctuations [*Bretherton et al*., 1992], the MCA identifies the embedded coupled time-space patterns by maximizing their covariance without a priori (Table 2). Therefore, it is very useful to detect possible cause-effect relationships between two parameters, particularly for climatic variables [*Ding et al*., 2011]. In this study, MCA is applied between austral extratropical precipitation and each climatic forcing factor to investigate their possible linkages.

3.2. ELM

ELM, an advanced machine learning tool, is proposed to improve learning speed and accuracy for the single hidden feedforward neural networks (SLFNs). The theoretical basis of ELM was detailed in *Huang et al*. [2006]. As suggested therein, the ELM works in a different way from traditional SLFNs learning algorithms, which need all the input weights and hidden layer biases to be adjusted and tuned, weights and biases are randomly assigned in ELM if the activation functions are infinitely differentiable while the hidden layer output matrix remains

unchanged. This advantage allows the ELM to respond to the given inputs directly and quickly find a solution for the designated problem without huge intervention, enabling better universal generalization performance with less training error. Due to its fast learning speed and fair accuracy, the ELM has been widely used for solving complex generalization problems and classification purposes [*Huang et al.*, 2012; *Bai et al.*, 2015; *Chang et al.*, 2015].

In this study, the ELM was applied to quantitatively simulate interactions between austral extratropical precipitation and four designated climatic forcing factors. In practice, precipitation time series extracted from MCA modes associated with each forcing factor were averaged to represent the overall precipitation changes during 1979–2013, and this mean precipitation time series was used as the target in ELM simulation processes. In addition, associated climatic forcing factor time series were taken as the inputs. Due to different magnitudes and units of forcing factors, all inputs were normalized beforehand to make them comparable. After normalization, all inputs and associated targets were randomly separated into two data sets, with 70% of them for model training and the rest for model testing, to guarantee the robustness and independence of the simulated models. Initially, the model was trained with the pair-wised 70% inputs and targets. Once the model was calibrated, the remaining inputs were used to predict the targets for model validation. Then, a correlation coefficient was calculated between the predicted data and the real targets. If this correlation coefficient is lower than the desired level (i.e., 0.9 in this study), the simulated model is not considered robust enough and the training process for model calibration will be repeated until the defined criterion is satisfied.

Once an acceptable ELM model can be established, a sensitivity analysis was conducted to estimate precipitation responses to each climatic forcing factor. In this study, two different numerical schemes were applied for sensitivity analysis. The first scheme toward estimating the precipitation responses to each forcing factor is designed to exclude one forcing factor from the input array at a time when dealing with the established model for precipitation prediction. The differential precipitation responses to that forcing factor can thus be quantified as differences between these two predicted precipitation time series. Taking the Antarctic ozone depletion as an example, the associated precipitation responses were estimated as

$$\mathrm{Precip}_{\mathrm{all}} = \Pi_t(\mathrm{O_3}, \mathrm{CO_2}, \mathrm{H_2O}, \mathrm{SST}) \tag{8}$$

$$\widehat{\mathrm{Precip}} = \Pi_t(\mathrm{CO_2}, \mathrm{H_2O}, \mathrm{SST}) \tag{9}$$

$$\mathrm{Precip}_{\mathrm{O_3}} = \mathrm{Precip}_{\mathrm{all}} - \widehat{\mathrm{Precip}}, \tag{10}$$

where $\mathrm{O_3}, \mathrm{CO_2}, \mathrm{H_2O}$, and SST represent climatic forcing of ozone, carbon dioxide, water vapor, and SST, respectively. $\mathrm{Precip}_{\mathrm{all}}$ denotes the predicted precipitation time series with having all four forcing factors included, while $\widehat{\mathrm{Precip}}$ represents the predicted precipitation time series without forcing from ozone. $\mathrm{Precip}_{\mathrm{O_3}}$ thus represents the differential precipitation responses to the forcing of ozone depletion. Similarly, precipitation responses to other forcing factors can also be estimated following the above scheme.

The other scheme is designed to replace each forcing factor with a new time series sequentially, in which the data values of each forcing factor are all prescribed to the value in 1979, while other time series vary with time. This scheme is dedicated to investigating differential precipitation responses to the variation of forcing factors after 1980. With this scheme, we can easily tell the increase or decrease of precipitation over the austral extratropics if there is no significant external forcing from Antarctic ozone depletion or global warming. Due to the random nature of ELM, multiple trials were conducted to establish fair accuracies. Ensemble means were applied to reduce stochastic biases from randomly established models. In this study, a total of 50 trials was conducted, and the uncertainties were characterized by two standard deviations (i.e., $\pm 2\sigma$) of these 50 trials outputs.

4. Results

Coupled MCA modes were derived to detect possible linkages between austral extratropical precipitation and each climatic forcing factor of interest. As shown in Figure 2, apparent moistening (i.e., increased precipitation) pattern was observed over the austral extratropics, along with significant ozone depletion over Antarctica, in particular over the East Antarctica, where TCO depleted more than 30 DU. In the temporal domain, it indicates a significant negative correlation (−0.78) between austral extratropical precipitation and TCO. The decreasing pattern of TCO clearly shows the dramatic ozone depletion in the past decades. Meanwhile, this coupled MCA mode explains a SCF of 90.8%, which suggests that the primary couplings between them are depleted TCO and increased precipitation. By the same way, couplings between austral extratropical precipitation

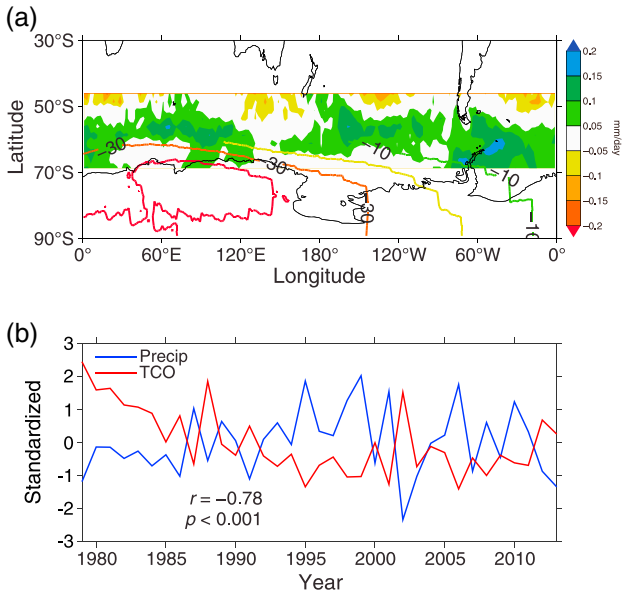

Figure 2. Coupled MCA mode between Antarctic ozone and the austral extratropical precipitation. (a) Spatial patterns of the first MCA mode between Antarctic TCO (contour line) and precipitation (shaded color). Total squared covariance explained by the first MCA mode is 90.8%. Note that all the Antarctic ozone shows a negative value (unit: DU) indicating dramatic ozone depletion over Antarctica. (b) Standardized time series (divided by its one standard deviation) of Antarctic total column ozone and associated austral extratropical precipitation extracted from the first MCA mode.

and global scale SST or water vapor were also investigated (Figure 3). Derived MCA modes indicate that the cooling of tropical Pacific Ocean (decreased SST in Figure 3b) and increased water vapor concentration in the atmosphere had resulted in apparent austral extratropical moistening. The two MCA modes explain a SCF of 35.22% (SST) and 44.38% (water vapor), respectively. Extracted principal time series from coupled MCA modes all show significant correlation between precipitation and each climatic forcing factor, which confirms the linkages between austral extratropical precipitation and each climatic forcing factor.

Since all the three climatic forcing factors have shown comparable correlations with austral extratropical precipitation, further quantifications should be conducted to investigate the predominant forcing factor in modulating the observed precipitation variations. As shown in Figure 4, there is no significant difference among principal precipitation time series derived from each coupled MCA mode. Therefore, an average of these time series was applied to represent the overall precipitation variability in the past decades. With the aid of ELM, statistical relationships between austral extratropical precipitation and each climatic forcing factor were established. It shows that the simulated precipitation time series agree well to the observed one via the ELM, with a correlation coefficient of 0.93 between them (Figure 5). With each well calibrated simulation model, it enables us to quantify precipitation responses to each forcing factor. As shown in Figure 6, precipitation responses to each forcing factor were indicated by ensemble means of relevant multiple trial outputs. These quantified precipitation responses clearly delineate the prominent forcing effect of each climatic factor. It is observed that the depleted Antarctic ozone and the increased GHGs (both carbon dioxide and water vapor) resulted in apparent precipitation increases over the austral extratropics (i.e., positive precipitation responses). Compared to other three forcing factors resulting in significant precipitation increase, SST mainly modulates positive and negative phases of the austral extratropical precipitation variability through the ocean-atmosphere interaction patterns, such as El Niño–Southern Oscillation and La Niña. Total precipitation responses were also calculated by adding each individual response together (Figure 7). It shows that the total precipitation responses agree well to the observed precipitation variability; however, slight overestimation is still observed, which suggests that these climatic forcing factors are not independent with each other when contributing to the observed precipitation variability.

To estimate the relative importance of each forcing factor contributing to the observed precipitation variability in the past decades, principal component analysis (PCA) was performed on the four precipitation responses. Results shown in Figure 8 clearly indicate the relative contribution of each forcing factor, with the primary forcing from Antarctic ozone depletion (explaining a total variance of 52.11%), followed by SST (35.75%), water vapor (9.43%), and carbon dioxide (2.71%). It shows a clear precipitation increase trend after Antarctic ozone depletion and a decreasing trend since 2006, from which the early signs of ozone recovery were observed [*Newman et al.*, 2006]. This derived precipitation response pattern is also fully in accordance with the observed precipitation variability in Figure 1, which indicates that the Antarctic ozone depletion had played a predominant role in triggering the observed austral extratropical moistening. In addition,

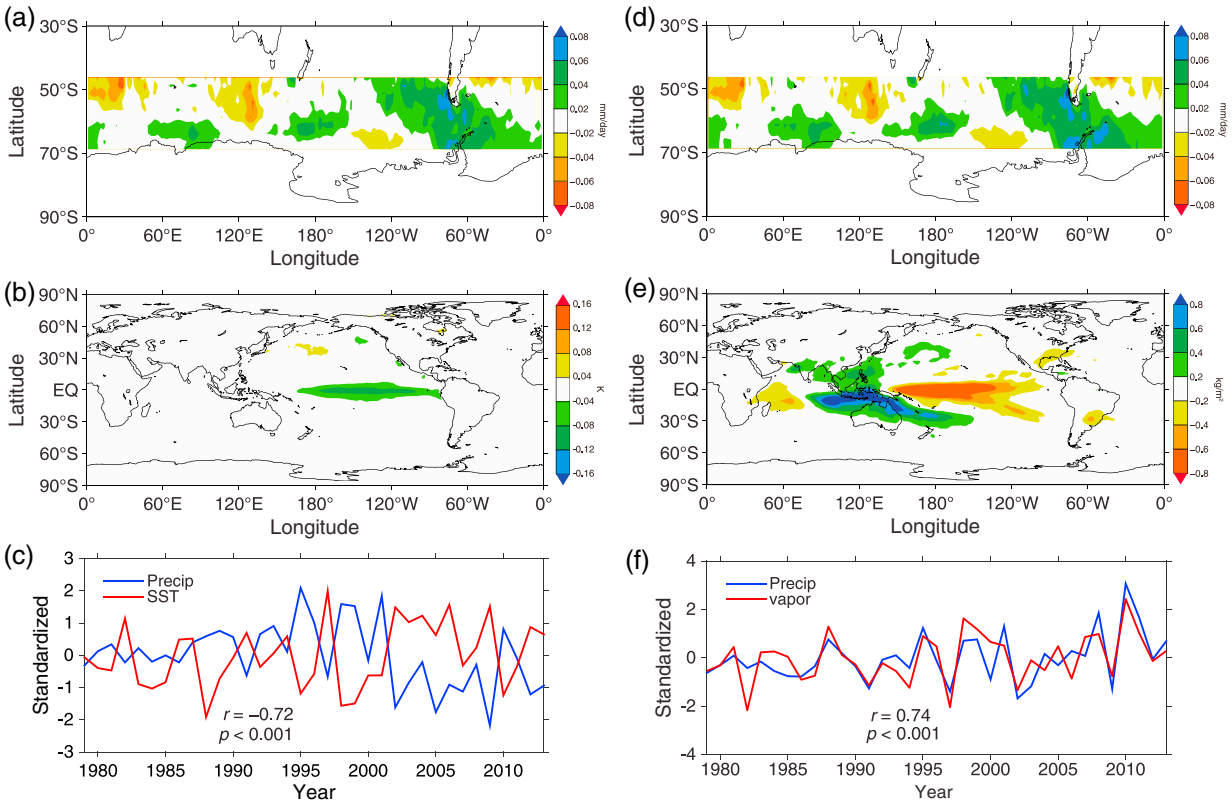

Figure 3. Same as in Figure 2 but for (a–c) SST and (d–f) water vapor. The SCF explained by these two MCA modes is 35.22% and 44.38%, respectively.

SST also played a critical role by modulating the interannual variability of austral extratropical precipitation, instead of contributing to the precipitation increases. It is observed that the increased GHGs in the atmosphere also contributed to the observed austral extratropical moistening; however, these contributions are very mild when comparing with those from other two forcing factors, in particular the Antarctic ozone depletion.

To further demonstrate the predominant role of Antarctic ozone depletion in triggering the observed austral extratropical moistening, the other sensitivity test was conducted numerically by quantifying precipitation responses to changing forcing since 1980, at which dramatic ozone depletion was observed over Antarctica. By specifying all data values in each forcing factor same as the one observed in 1979 sequentially,

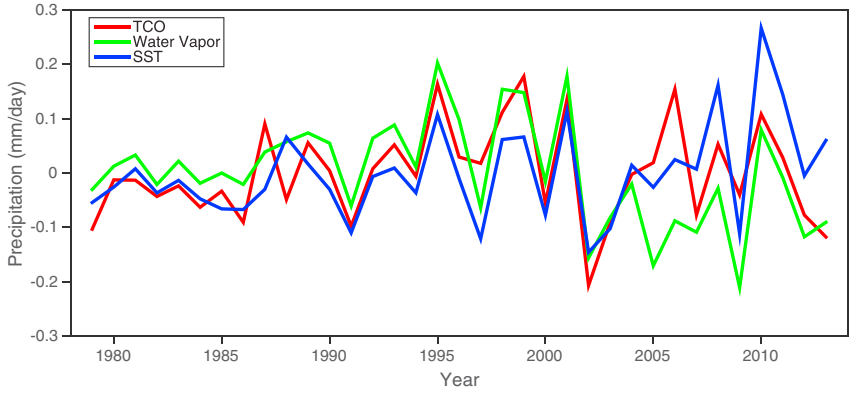

Figure 4. Comparisons of derived precipitation time series associated with each forcing factor from the coupled MCA modes. An average of these time series was applied to represent the overall precipitation variability over austral extratropics during 1979–2013 and was used as targets in further modeling processes in this study.

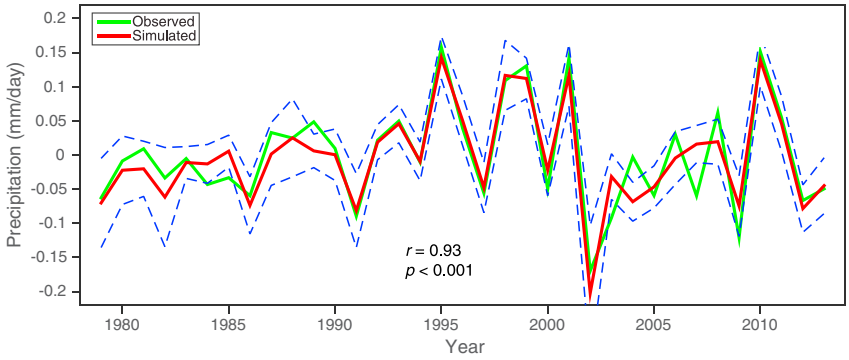

Figure 5. Comparisons between observed and simulated precipitation time series. The simulated time series are ensemble means of 50 trials outputs. Uncertainties are characterized by two standard deviations (± 2σ) of these 50 simulations.

precipitation responses to each forcing factor can be estimated from the differences between two predicted precipitation time series (equation (10)). As shown in Figure 9, by setting each forcing factor to be its pre-1980 level, only the precipitation response to Antarctic ozone shows an apparent decrease pattern, which suggests that a decline of precipitation would be observed over austral extratropics without the presence of the forcing from Antarctic ozone depletion. In addition, results from principal component analysis (Figure 10) show that the estimated precipitation responses to Antarctic ozone explains a total variance of 85.57% among all the four precipitation responses, with the remaining part explained by SST (10.23%) and GHGs (4.2%). These results are consistent with those from the first sensitivity scheme shown in Figure 8, which clearly demonstrate the predominant role of Antarctic ozone depletion in triggering the observed austral extratropical moistening, except slight differences in the explained variance. Nevertheless, there is no significant difference in the relative role of each forcing factor contributing to the observed austral extratropical moistening. In general, the observed moistening over austral extratropics can be primarily attributed to the dramatic

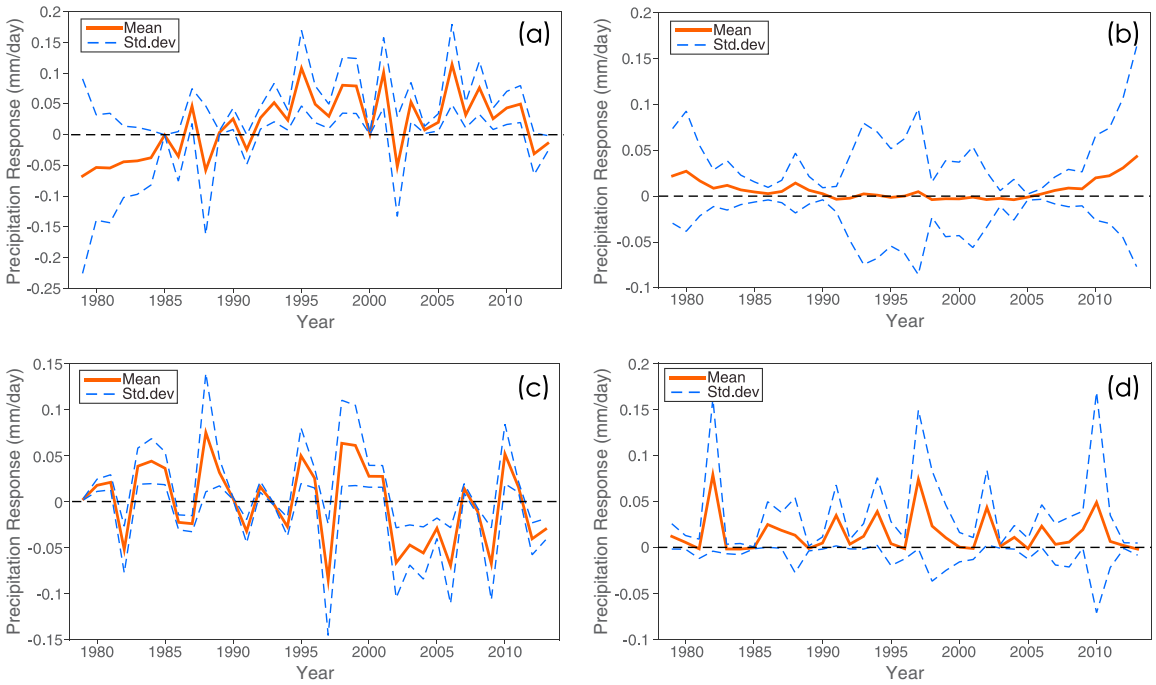

Figure 6. Austral extratropical precipitation responses to each climatic forcing factor by dropping that factor out of the modeling inputs. (a) Precipitation responses to forcing from Antarctic ozone depletion. (b) Precipitation responses to forcing from carbon dioxide. (c) Precipitation responses to forcing from SST. (d) Precipitation responses to forcing from water vapor. Uncertainties are characterized by two standard deviations (± 2σ) of 50 simulations.

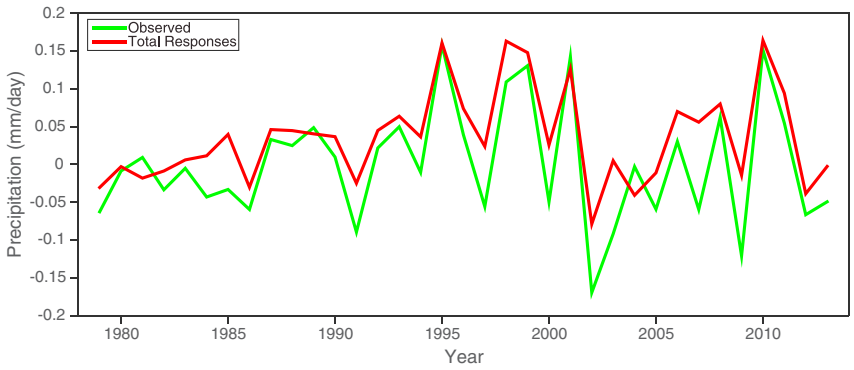

Figure 7. Comparisons between the observed precipitation variability and the total simulated precipitation responses. Total precipitation responses are summations of the four individual responses (ensemble mean) in Figure 6.

ozone depletion over Antarctica, as the variability of this moistening is also modulated by the cooling phase of SST over tropical Pacific Ocean and increased GHGs in the atmosphere.

To further justify the linkage between Antarctic ozone depletion and the observed austral extratropical moistening, couplings between Antarctic ozone depletion and austral zonal wind were investigated. As shown in Figure 11, the first MCA mode has explained a total covariance of 96.2% between these two variables. The coupled time-space patterns clearly indicate an intensified zonal wind over the austral extratropics being associated with Antarctic ozone depletion, which is also in full accordance with the observed zonal wind changes before and after significant ozone decline over Antarctica (Figure 11a). As indicated there, a poleward shift of the atmospheric circulation is observed after the ozone decline. The agreement between the observed and the coupled patterns suggests that the observed poleward shift of the atmospheric circulation in the SH should be primarily attributed to dramatic ozone depletion over Antarctica. This detected coupling is also consistent with other modeling results, which suggest an inherent linkage that the ozone depletion had altered the circulation pattern in the SH, by favoring a poleward shifting westerly jet, which

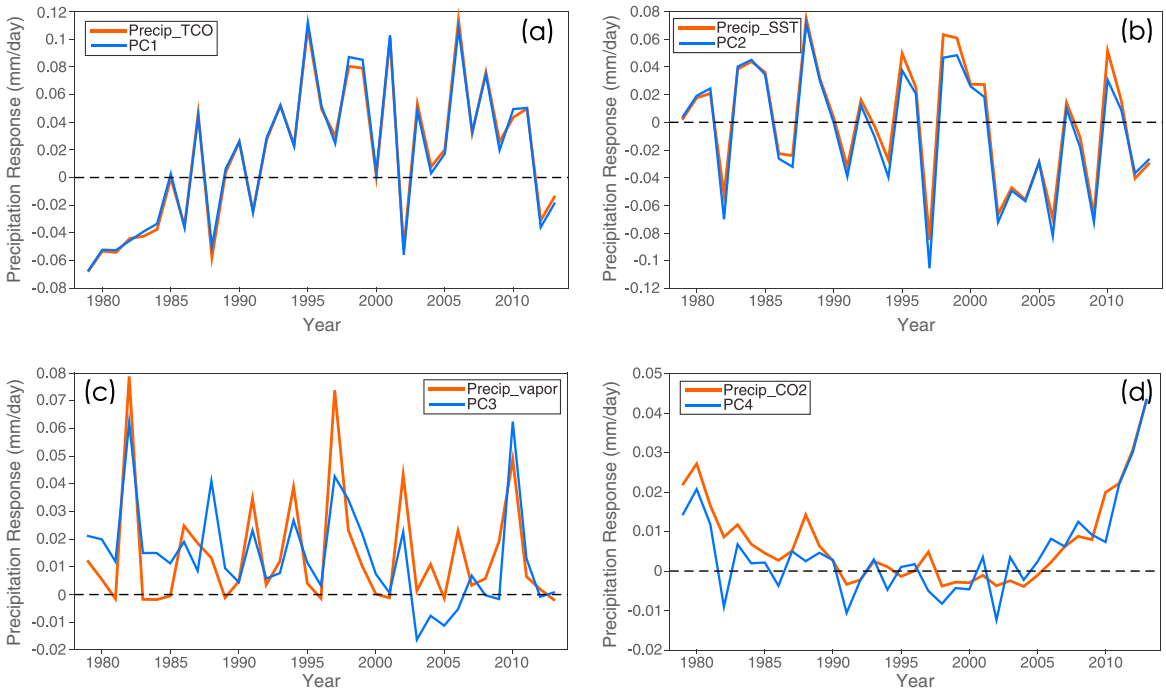

Figure 8. Comparison of principal components and the associated precipitation responses. Explained variances by four principal components are 52.11%, 35.75%, 9.43%, and 2.71%, respectively.

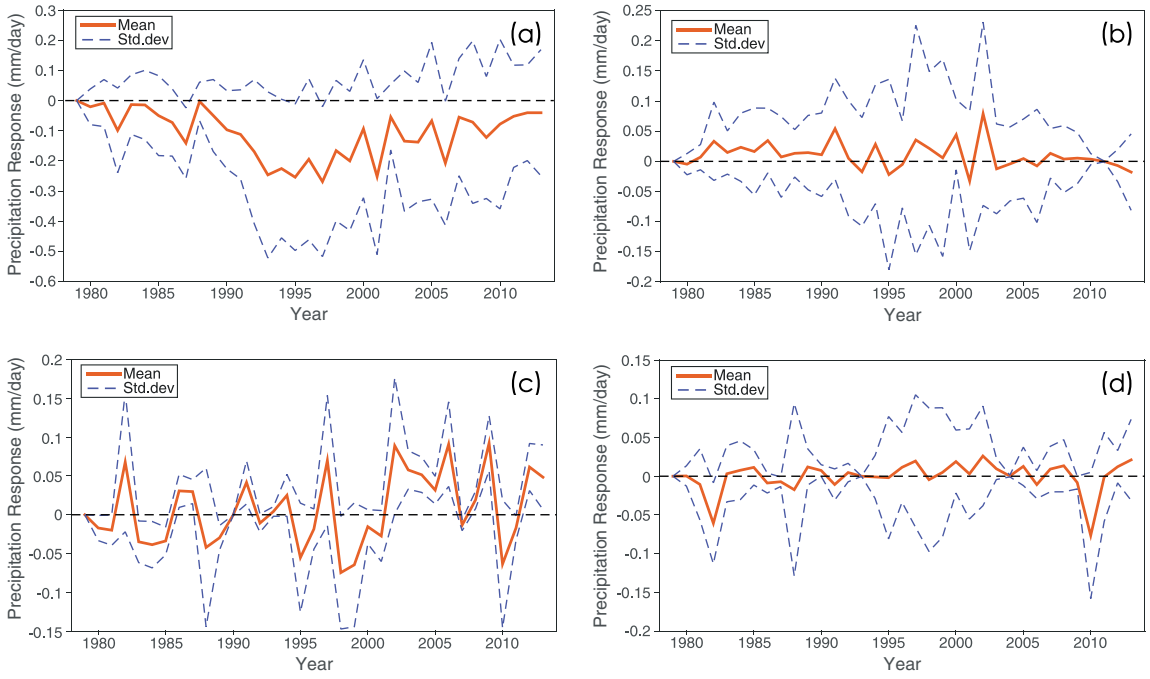

Figure 9. Austral extratropical precipitation responses to each climatic forcing factor by keeping each forcing factor being constant to its 1979 level. (a) Precipitation responses to forcing from Antarctic ozone depletion. (b) Precipitation responses to forcing from carbon dioxide. (c) Precipitation responses to forcing from SST. (d) Precipitation responses to forcing from water vapor. Uncertainties are characterized by two standard deviations ($\pm 2\sigma$) of 50 simulations.

in turn resulted in apparent regional climatic changes [*Son et al.*, 2010; *Kang et al.*, 2011, 2013]. As suggested by *Perlwitz* [2011], a cooling of the polar stratosphere is observed after the depletion of ozone owing to the reduced absorption of ultraviolet radiation. This cooling in turn leads to a delayed austral summertime response in the lower atmosphere, characterized by a poleward shift of the jet stream that is associated with

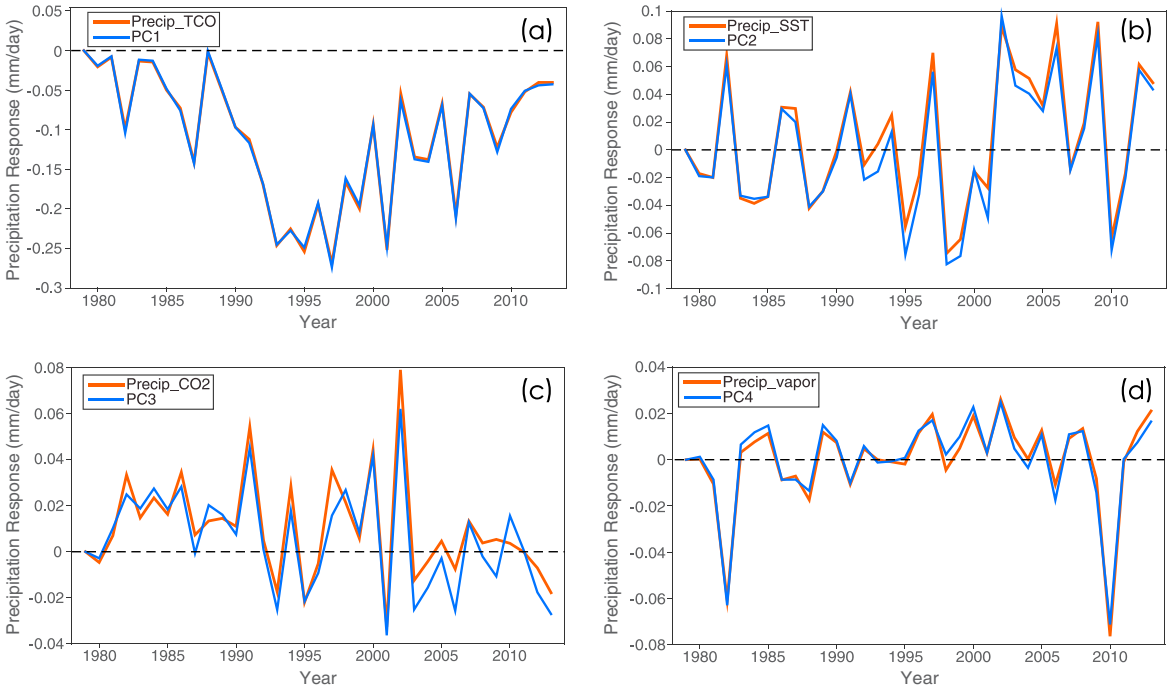

Figure 10. Comparison of principal components and the associated precipitation responses in Figure 9. Explained variances by these four principal components are 85.57%, 10.23%, 2.43%, and 1.77%, respectively.

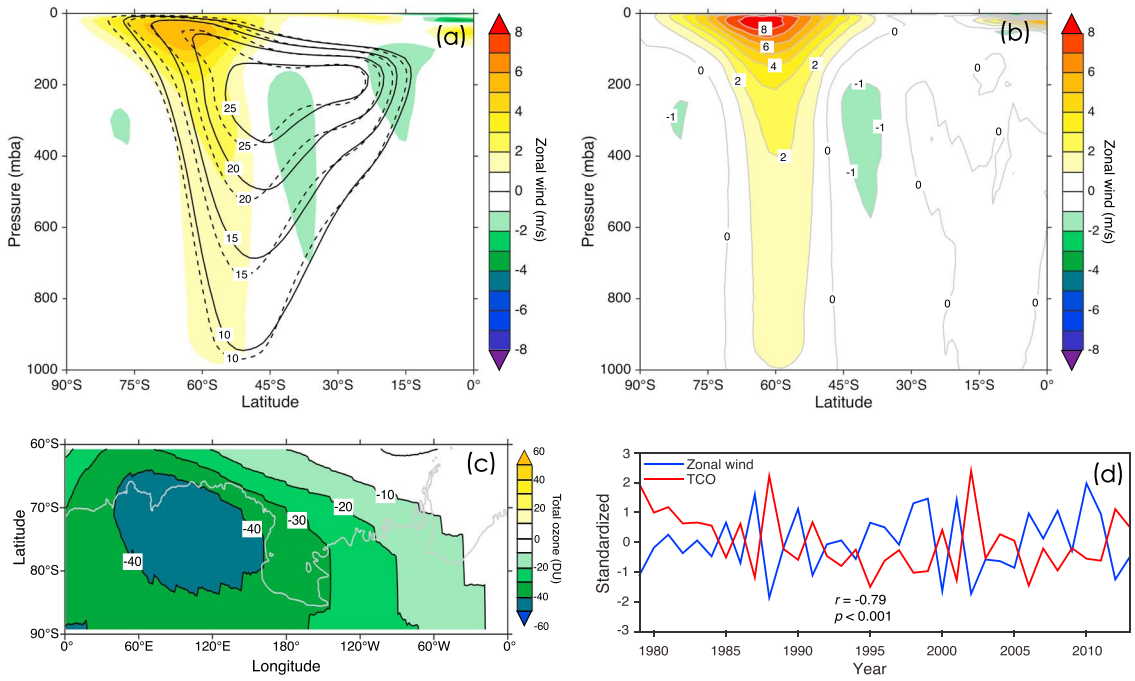

Figure 11. Coupled patterns between austral zonal mean zonal wind and Antarctic ozone depletion. (a) Observed zonal mean zonal wind changes before and after the formation of large ozone hole, (b) the first MCA mode of zonal wind changes coupled with Antarctic ozone depletion, (c) the first MCA model of TCO over Antarctica, and (d) standardized time series of TCO and zonal wind extracted from the first MCA mode. Contour lines in Figure 11a represent the zonal mean zonal wind before (solid line) and after (dashed line) large ozone hole formed. The first MCA mode explains a total covariance of 96.2% between zonal mean zonal wind and Antarctic ozone depletion.

westerly winds at midlatitudes. The direct consequences of this shift are weather and climate changes at the surface, because the jet stream determines the tracks of storms at middle-and-high latitudes.

5. Discussion

In this study, two empirical approaches were applied to investigate the relative contribution of Antarctic ozone depletion to further justify its predominant role in triggering the observed austral extratropical moistening. In addition to the forcing from Antarctica ozone depletion, another three climatic forcing factors, including SST, carbon dioxide, and water vapor, were employed to compare with Antarctica ozone depletion. Quantified precipitation response to each climatic forcing factor suggests the predominant role of Antarctic ozone depletion in triggering the observed austral extratropical moistening. This finding provides distinctive evidence to justify the previous conflicting results from various climatic modeling analyses. As suggested in the literature, the observed SH climatic changes resulted mainly from the joint effects of Antarctic ozone depletion and increasing GHGs in the atmosphere. However, in this study, results from both two numerical schemes for sensitivity test manifest the equatorial Pacific cooling (i.e., decreasing SST) had played a relative more important role than GHGs in modulating the austral extratropical precipitation variability, in addition to the predominant forcing from Antarctic ozone depletion. In this context, the relative contribution of GHGs is even negligible. These detected couplings highlight the importance of equatorial Pacific SST anomalies in modulating regional climatic changes in the SH, suggesting that the relative role of equatorial Pacific SST anomalies should be considered and well characterized in climate models for accurate prediction of future climate in the SH. Evidences toward the impact of equatorial Pacific SST anomalies on the SH climate can be found in studies such as *Ding et al*. [2011] and *Kosaka and Xie* [2013].

Due to the lack of global scale gridded long-term carbon dioxide observations, monthly carbon dioxide records at Mauna Loa were used as representative data to diagnose the possible forcing effects of increasing carbon dioxide concentrations in the atmosphere. A potential GHG was also applied to include the possible forcing from GHGs. However, quantified precipitation responses to these two factors (i.e., carbon dioxide and GHGs) are very small, even negligible, compared with those from Antarctic ozone depletion and cooling of

equatorial Pacific. Compared to climatic modeling results, the relative role of GHGs seems to be underestimated in this study. To some extent, it could be attributed to insufficient forcing from carbon dioxide due to the lack of global scale coverage. However, comparisons of coupled precipitation to water vapor and other two forcing factors (i.e., Antarctic ozone depletion and equatorial Pacific SST) indicate small differences among them (Figure 4), which in turn suggests that these forcing factors are fairly comparable to each other. Therefore, the sensitivity tests in this study should explain most of the differential contribution of each forcing factor to the observed austral extratropical precipitation variability, with little to be left to other unknown factors. This can be deduced from comparisons between water vapor and SST, as water vapor has a closer cause-effect relationship with the austral extratropical precipitation than that of SST (i.e., higher correlation value in Figure 3); however, the quantified precipitation responses indicate that the SST has a more significant contribution than water vapor in this regard.

In this study, only four climatic forcing factors were considered. In addition to these factors, other internal and external forcing factors could contribute to the observed austral extratropical precipitation changes. Clouds and aerosols, which have significant climate effects by perturbing the atmospheric radiation budget, may also played a role in triggering this wetting climate [e.g., *Dessler*, 2010; *Mahowald*, 2011; *Rosenfeld et al*., 2014]. Volcanic eruptions, which change the atmosphere structure by ejecting large amounts of dust and ash into the atmosphere, force climate changes in a similar way as aerosols [e.g., *Muthers et al*., 2014]. Solar variability, a natural forcing factor from the sun, is also capable of modulating global climate, despite its small direct impact at the Earth's surface [e.g., *Ricke et al*., 2010; *Varma et al*., 2011]. Anthropogenic land use and land cover changes are also observed to affect global climate by altering the ground surface albedo [e.g., *Pielke et al*., 2011]. However, owing to the lack of long-term global data sources and the prior knowledge of the possible primary forcing factors in modulating the SH climate, aforementioned factors are not considered in this study, and their relative contributions to the observed austral extratropical moistening remain unclear, which require further scientific investigations.

In regard to uncertainties embedded in our final results, some of them could arise from the derived coupled time-space patterns between austral extratropical precipitation and each climatic forcing factor. Since the MCA works relying on detecting principal coupled modes with respect to maximum covariance, the extracted MCA modes can only realize the leading pattern of each variable, while leaving out some other varying patterns. Nevertheless, these discarded patterns may be considered as noise relative to the leading coupled patterns and will not significantly affect our final results. However, uncertainties from statistical modeling processes are critical. In this study, ELM was applied to establish the quantitative cause-effect relationships between austral extratropical precipitation variations and relevant climatic forcing factors. Due to the stochastic nature of ELM, each simulated model could be different from the previous one; hence, multiple models were simulated to gain a high level of confidence and to avoid randomly determined contribution of each forcing factor. For example, if one forcing factor is not highly related to the precipitation changes, the weights assigned to it in training an ELM model may vary with large fluctuations. This effect can be observed from the large standard deviation of the precipitation response to carbon dioxide in Figure 6b. Additionally, toward each simulated model, the training inputs were different due to the random inputs assignment strategy to avoid occasional data dependent model simulations. Moreover, uncertainties could also arise from quantifying differential contributions of each forcing factor. The differential contributions of forcing factors were computed based on the similarity between each original precipitation response and associated principal components. Therefore, uncertainties may arise here from incomplete and misaligned overlapping range of the principal components within the original time series, such as the comparison of the PC3 and water vapor-associated precipitation responses (Figure 6c). Nevertheless, fair agreements between the PC1 and the precipitation responses to Antarctic ozone depletion strongly suggest the predominant role of Antarctic ozone depletion in triggering the observed SH extratropical moistening.

In addition, as shown in both Figures 6a and 9a, different precipitation responses to ozone depletion are observed. Results indicate an increased precipitation trend varying with extended size of Antarctic ozone hole. However, this pattern may be reversed after the recovery of Antarctic ozone hole, which can be even observed from the decreased precipitation responses since 2006, when the early signs of ozone recovery are detected. As suggested here and documented in other studies, the observed climatic changes in the SH should be primarily attributed to the joint effects of Antarctic ozone depletion and increase in GHGs concentrations, being dominated by the Antarctic ozone depletion. Therefore, with the recovery of the ozone

hole in the SH over upcoming decades [*WMO*, 2011, 2014], these joint effects may stabilize, decrease, or even reverse. Modeling experiments suggest that the ozone recovery will oppose and cancel out the climatic forcing from rising GHGs concentrations in the atmosphere, which in turn may result in global scale tropospheric warming [e.g., *Hu et al*., 2011], negative summertime trends in the Southern Annular Mode [e.g., *Arblaster et al*., 2011], reversed tropospheric circulation changes [e.g., *Perlwitz et al*., 2008], and a delay in summertime SH climate change characterized by significantly reduced trends in the position of the jet stream, the width of the subtropical dry zones, the seasonality of surface temperatures, and sea ice concentrations [e.g., *Barnes et al*., 2014]. However, to what extent the recovery of the ozone hole will cancel out climatic forcing from rising GHGs remains unclear, which primarily depends on the competing effect of the rate of ozone hole recovery and GHGs emissions. A faster recovery of the ozone hole would cause an equatorward jet stream, while a larger increasing rate of GHGs would tend to drive the jet stream moving poleward [*Perlwitz*, 2011]. Therefore, a clear understanding of climatic responses to the relative forcing factors is critical to accurate prediction of future changing climate.

6. Summary and Conclusions

To demonstrate the predominant role of Antarctic ozone depletion in triggering the observed austral extratropical moistening, precipitation responses to each predetermined climatic forcing factors were quantitatively estimated through a statistical modeling process. Quantified precipitation responses indicate that the observed austral extratropical precipitation increase should be primarily attributed to the dramatic ozone depletion over Antarctica, as more than half of the total precipitation variations can be explained by the depleted TCO over Antarctica. In addition to the Antarctic ozone depletion, the cooling phase of equatorial Pacific SST is also deemed as an important role in modulating precipitation changes over the austral extratropics. When compared to these two leading forcing factors, GHGs are observed to play a relatively weak role. These findings provide additional evidence to confirm the competing role of Antarctic ozone depletion and increasing GHGs concentrations in modulating changing climates in the SH. In general, our findings can be summarized as follows. (1) The MCA works efficiently in detecting relevant couplings between two climatic variables and is helpful in investigating the inherent mechanisms from large scale interactions. (2) Quantified precipitation responses to each climatic forcing factor prioritize the predominant role of Antarctic ozone depletion in triggering the observed austral extratropical moistening. (3) Differing from climatic modeling outputs, which indicate that the changing climate in the SH should be mainly attributed to the joint effects of Antarctic ozone depletion and increasing GHGs, the relatively stronger role of equatorial Pacific SST anomalies is highlighted in this study, suggesting the need to consider this climatic forcing factor in predicting future climate scenarios.

Overall, this study demonstrates an inductive approach to rank the predominant role of Antarctic ozone depletion when compared to the other three climatic forcing factors, particularly the GHGs, in triggering the observed moistening pattern over the austral extratropics. The findings here provide additional evidences to harmonize the conflicting results between climatic modeling outputs, which also provide valuable hypotheses for future climate modeling analyses. With these hypotheses, for instance, the physical mechanism of the equatorial Pacific SST in modulating the SH climate should be further investigated in future climatic modeling experiments.

Acknowledgments
The GPCP Version 2.2 Combination Data were obtained from the NASA Goddard Space Flight Center, the ERA-Interim Reanalysis data from the ECMWF, and the carbon dioxide data from the NOAA/ESRL. This work was supported by the Science and Technology Commission of Shanghai Municipality (15dz1207805 and 13231203804) and USDA NIFA (2015-34263-24070).

References

Abdi, H., and L. J. Williams (2010), Principal component analysis, *Wiley Interdiscip. Rev. Comput. Stat.*, *2*(4), 433–459, doi:10.1002/wics.101.

Adler, R. F., et al. (2003), The version-2 Global Precipitation Climatology Project (GPCP) monthly precipitation analysis (1979–present), *J. Hydrometeorol.*, *4*(6), 1147–1167, doi:10.1175/1525-7541(2003)004<1147:TVGPCP>2.0.CO;2.

Antón, M., M. López, J. M. Vilaplana, M. Kroon, R. McPeters, M. Bañón, and A. Serrano (2009), Validation of OMI-TOMS and OMI-DOAS total ozone column using five Brewer spectroradiometers at the Iberian peninsula, *J. Geophys. Res.*, *114*, D14307, doi:10.1029/2009JD012003.

Arblaster, J. M., G. A. Meehl, and D. J. Karoly (2011), Future climate change in the Southern Hemisphere: Competing effects of ozone and greenhouse gases, *Geophys. Res. Lett.*, *38*, L02701, doi:10.1029/2010GL045384.

Bai, K., N.-B. Chang, and C.-F. Chen (2015), Spectral Information Adaptation and Simulation Scheme (SIASS) for merging cross-mission consistent ocean color reflectance observations from MODIS and VIIRS, *IEEE Trans. Geosci. Remote Sens.*, *1–19*, doi:10.1109/TGRS.2015.2456906.

Barnes, E. A., N. W. Barnes, and L. M. Polvani (2014), Delayed Southern Hemisphere climate change induced by stratospheric ozone recovery, as projected by the CMIP5 models, *J. Clim.*, *27*(2), 852–867, doi:10.1175/JCLI-D-13-00246.1.

Barnett, T., F. Zwiers, G. Hegerl, and M. Allen (2005), Detecting and attributing external influences on the climate system: A review of recent advances, *J. Clim.*, *18*(9), 1291–1314, doi:10.1175/JCLI3329.1.

Bretherton, C. S., C. Smith, and J. M. Wallace (1992), An intercomparison of methods for finding coupled patterns in climate data, *J. Clim.*, *5*(6), 541–560, doi:10.1175/1520-0442(1992)005<0541:AIOMFF>2.0.CO;2.

Bromwich, D. H., J. P. Nicolas, A. J. Monaghan, M. A. Lazzara, L. M. Keller, G. A. Weidner, and A. B. Wilson (2012), Central West Antarctica among the most rapidly warming regions on Earth, *Nat. Geosci.*, *6*(2), 139–145, doi:10.1038/ngeo1671.

Buermann, W., B. R. Lintner, C. D. Koven, A. Angert, J. E. Pinzon, C. J. Tucker, and I. Y. Fung (2007), The changing carbon cycle at Mauna Loa Observatory, *Proc. Natl. Acad. Sci. U. S. A.*, *104*(11), 4249–4254, doi:10.1073/pnas.0611224104.

Cariolle, D., and H. Teyssèdre (2007), A revised linear ozone photochemistry parameterization for use in transport and general circulation models: Multi-annual simulations, *Atmos. Chem. Phys.*, *7*(9), 2183–2196, doi:10.5194/acp-7-2183-2007.

Cariolle, D., and M. Déqué (1986), Southern hemisphere medium-scale waves and total ozone disturbances in a spectral general circulation model, *J. Geophys. Res.*, *91*(D10), 10,825–10,846, doi:10.1029/JD091iD10p10825.

Chang, N.-B., K. Bai, and C.-F. Chen (2015), Smart information reconstruction via time-space-spectrum continuum for cloud removal in satellite images, *IEEE J. Sel. Top. Appl. Earth Obs. Remote Sens.*, doi:10.1109/JSTARS.2015.2400636.

Dee, D. P., et al. (2011), The ERA-Interim reanalysis: Configuration and performance of the data assimilation system, *Q. J. R. Meteorol. Soc.*, *137*(656), 553–597, doi:10.1002/qj.828.

Dee, D., and S. Uppala (2009), Variational bias correction of satellite radiance data in the ERA-Interim reanalysis, *Q. J. R. Meteorol. Soc.*, *135*(644), 1830–1841, doi:10.1002/qj.493.

Delworth, T. L., F. Zeng, and G. Noaa (2014), Regional rainfall decline in Australia attributed to anthropogenic greenhouse gases and ozone levels, *Nat. Geosci.*, *7*(8), 583–587, doi:10.1038/ngeo2201.

Dessler, A. E. (2010), A determination of the cloud feedback from climate variations over the past decade, *Science*, *330*, 1523–1527, doi:10.1126/science.1192546.

Dethof, A., and E. V. Hólm (2004), Ozone assimilation in the ERA-40 reanalysis project, *Q. J. R. Meteorol. Soc.*, *130*(603), 2851–2872, doi:10.1256/qj.03.196.

Dhanya, C. T., and D. Nagesh Kumar (2009), Data mining for evolution of association rules for droughts and floods in India using climate inputs, *J. Geophys. Res.*, *114*, D02102, doi:10.1029/2008JD010485.

Ding, Q., E. J. Steig, D. S. Battisti, and M. Küttel (2011), Winter warming in West Antarctica caused by central tropical Pacific warming, *Nat. Geosci.*, *4*(6), 398–403, doi:10.1038/ngeo1129.

Dragani, R. (2011), On the quality of the ERA-Interim ozone reanalyses: Comparisons with satellite data, *Q. J. R. Meteorol. Soc.*, *137*(658), 1312–1326, doi:10.1002/qj.821.

Eyring, V., et al. (2013), Long-term ozone changes and associated climate impacts in CMIP5 simulations, *J. Geophys. Res. Atmos.*, *118*, 5029–5060, doi:10.1002/jgrd.50316.

Feldstein, S. B. (2011), Subtropical rainfall and the Antarctic ozone hole, *Science*, *332*(6032), 925–926, doi:10.1126/science.1206834.

Forster, P., et al. (2007), Changes in atmospheric constituents and in radiative forcing, in *Climate Change 2007: The Physical Science Basis*, edited by S. Solomon et al., pp. 131–215, Cambridge Univ. Press, Cambridge.

Fyfe, J. C., N. P. Gillett, and G. J. Marshall (2012), Human influence on extratropical Southern Hemisphere summer precipitation, *Geophys. Res. Lett.*, *39*, L23711, doi:10.1029/2012GL054199.

Gonzalez, P. L. M., L. M. Polvani, R. Seager, and G. J. P. Correa (2013), Stratospheric ozone depletion: A key driver of recent precipitation trends in South Eastern South America, *Clim. Dyn.*, *42*(7–8), 1775–1792, doi:10.1007/s00382-013-1777-x.

Hasselmann, K. (1998), Conventional and Bayesian approach to climate-change detection and attribution, *Q. J. R. Meteorol. Soc.*, *124*(552), 2541–2565, doi:10.1256/smsqj.55201.

Hegerl, G. C., H. von Storch, K. Hasselmann, B. D. Santer, U. Cubasch, and P. D. Jones (1996), Detecting greenhouse-gas-induced climate change with an optimal fingerprint method, *J. Clim.*, *9*(10), 2281–2306, doi:10.1175/1520-0442(1996)009<2281:DGGICC>2.0.CO;2.

Hu, Y., Y. Xia, and Q. Fu (2011), Tropospheric temperature response to stratospheric ozone recovery in the 21st century, *Atmos. Chem. Phys.*, *11*(15), 7687–7699, doi:10.5194/acp-11-7687-2011.

Huang, G.-B., Q.-Y. Zhu, and C.-K. Siew (2006), Extreme learning machine: Theory and applications, *Neurocomputing*, *70*(1–3), 489–501, doi:10.1016/j.neucom.2005.12.126.

Huang, G.-B., H. Zhou, X. Ding, and R. Zhang (2012), Extreme learning machine for regression and multiclass classification, *IEEE Trans. Syst. Man. Cybern. B*, *42*(2), 513–529, doi:10.1109/TSMCB.2011.2168604.

Huffman, G. J., R. F. Adler, D. T. Bolvin, and G. Gu (2009), Improving the global precipitation record: GPCP version 2.1, *Geophys. Res. Lett.*, *36*, L17808, doi:10.1029/2009GL040000.

Kang, S. M., L. M. Polvani, J. C. Fyfe, and M. Sigmond (2011), Impact of polar ozone depletion on subtropical precipitation, *Science*, *332*(6032), 951–954, doi:10.1126/science.1202131.

Kang, S. M., L. M. Polvani, J. C. Fyfe, S.-W. W. Son, M. Sigmond, G. J. P. Correa, G. J. P. Correa, and G. J. P. Correa (2013), Modeling evidence that ozone depletion has impacted extreme precipitation in the austral summer, *Geophys. Res. Lett.*, *40*, 4054–4059, doi:10.1002/grl.50769.

Kosaka, Y., and S.-P. Xie (2013), Recent global-warming hiatus tied to equatorial Pacific surface cooling, *Nature*, *501*(7467), 403–407, doi:10.1038/nature12534.

Mahowald, N. (2011), Aerosol indirect effect on biogeochemical cycles and climate, *Science*, *334*(6057), 794–796, doi:10.1126/science.1207374.

Manatsa, D., Y. Morioka, S. K. Behera, T. Yamagata, and C. H. Matarira (2013), Link between Antarctic ozone depletion and summer warming over southern Africa, *Nat. Geosci.*, *6*(11), 934–939, doi:10.1038/ngeo1968.

McLandress, C., A. I. Jonsson, D. A. Plummer, M. C. Reader, J. F. Scinocca, and T. G. Shepherd (2010), Separating the dynamical effects of climate change and ozone depletion. Part I: Southern Hemisphere stratosphere, *J. Clim.*, *23*(18), 5002–5020, doi:10.1175/2010JCLI3586.1.

McPeters, R., M. Kroon, G. Labow, E. Brinksma, D. Balis, I. Petropavlovskikh, J. P. Veefkind, P. K. Bhartia, and P. F. Levelt (2008), Validation of the Aura Ozone Monitoring Instrument total column ozone product, *J. Geophys. Res.*, *113*, D15S14, doi:10.1029/2007JD008802.

Muthers, S., et al. (2014), Northern hemispheric winter warming pattern after tropical volcanic eruptions: Sensitivity to the ozone climatology, *J. Geophys. Res. Atmos.*, *119*, 1340–1355, doi:10.1002/2013JD020138.

Newman, P. A., E. R. Nash, S. R. Kawa, S. A. Montzka, and S. M. Schauffler (2006), When will the Antarctic ozone hole recover? *Geophys. Res. Lett.*, *33*, L12814, doi:10.1029/2005GL025232.

Niranjan Kumar, K., and T. B. M. J. Ouarda (2014), Precipitation variability over UAE and global SST teleconnections, *J. Geophys. Res. Atmos.*, *119*, 10,313–10,322, doi:10.1002/2014JD021724.

Perlwitz, J. (2011), Atmospheric science: Tug of war on the jet stream, *Nat. Clim. Change*, *1*(1), 29–31, doi:10.1038/nclimate1065.

Perlwitz, J., S. Pawson, R. L. Fogt, J. E. Nielsen, and W. D. Neff (2008), Impact of stratospheric ozone hole recovery on Antarctic climate, *Geophys. Res. Lett.*, *35*, 1–5, doi:10.1029/2008GL033317.

Pielke, R. A., et al. (2011), Land use/land cover changes and climate: Modeling analysis and observational evidence, *Wiley Interdiscip. Rev. Clim. Change*, *2*(6), 828–850, doi:10.1002/wcc.144.

Previdi, M., and L. M. Polvani (2014), Climate system response to stratospheric ozone depletion and recovery, *Q. J. R. Meteorol. Soc.*, *140*(685), 2401–2419, doi:10.1002/qj.2330.
Ricke, K. L., M. G. Morgan, and M. R. Allen (2010), Regional climate response to solar-radiation management, *Nat. Geosci.*, *3*, 537–541, doi:10.1038/ngeo915.
Rosenfeld, D., S. Sherwood, R. Wood, and L. Donner (2014), Atmospheric science. Climate effects of aerosol-cloud interactions, *Science*, *343*(6169), 379–380, doi:10.1126/science.1247490.
Shaw, T. A., J. Perlwitz, N. Harnik, P. A. Newman, and S. Pawson (2011), The impact of stratospheric ozone changes on downward wave coupling in the Southern Hemisphere, *J. Clim.*, *24*(16), 4210–4229, doi:10.1175/2011JCLI4170.1.
Sigmond, M., and J. C. Fyfe (2014), The Antarctic sea ice response to the ozone hole in climate models, *J. Clim.*, *27*(3), 1336–1342, doi:10.1175/JCLI-D-13-00590.1.
Son, S.-W., L. M. Polvani, D. W. Waugh, H. Akiyoshi, R. Garcia, D. Kinnison, S. Pawson, E. Rozanov, T. G. Shepherd, and K. Shibata (2008), The impact of stratospheric ozone recovery on the Southern Hemisphere westerly jet, *Science*, *320*(5882), 1486–1489, doi:10.1126/science.1155939.
Son, S.-W., N. F. Tandon, L. M. Polvani, and D. W. Waugh (2009), Ozone hole and Southern Hemisphere climate change, *Geophys. Res. Lett.*, *36*, L15705, doi:10.1029/2009GL038671.
Son, S.-W., et al. (2010), Impact of stratospheric ozone on Southern Hemisphere circulation change: A multimodel assessment, *J. Geophys. Res.*, *115*, D00M07, doi:10.1029/2010JD014271.
Steinbach, M., P. Tan, and V. Kumar (2001), Clustering earth science data: Goals, issues and results, *Proc. of the Fourth KDD Workshop on Mining Scientific Datasets*.
Thoning, K. W., P. P. Tans, and W. D. Komhyr (1989), Atmospheric carbon dioxide at Mauna Loa Observatory: 2. Analysis of the NOAA GMCC data, 1974–1985, *J. Geophys. Res.*, *94*(D6), 8549–8565, doi:10.1029/JD094iD06p08549.
Tippett, M. K., T. DelSole, S. J. Mason, and A. G. Barnston (2008), Regression-based methods for finding coupled patterns, *J. Clim.*, *21*(17), 4384–4398, doi:10.1175/2008JCLI2150.1.
Varma, V., M. Prange, F. Lamy, U. Merkel, and M. Schulz (2011), Solar-forced shifts of the Southern Hemisphere Westerlies during the Holocene, *Clim. Past*, *7*, 339–347, doi:10.5194/cp-7-339-2011.
Wallace, J. M., C. Smith, and C. S. Bretherton (1992), Singular value decomposition of wintertime sea surface temperature and 500-mb height anomalies, *J. Clim.*, *5*(6), 561–576, doi:10.1175/1520-0442(1992)005<0561:SVDOWS>2.0.CO;2.
Waugh, D. W., L. Oman, P. A. Newman, R. S. Stolarski, S. Pawson, J. E. Nielsen, and J. Perlwitz (2009), Effect of zonal asymmetries in stratospheric ozone on simulated Southern Hemisphere climate trends, *Geophys. Res. Lett.*, *36*, L18701, doi:10.1029/2009GL040419.
World Meteorological Organization (WMO) (2011), Scientific assessment of ozone depletion: 2010, *Glob. Ozone Res. and Monit. Proj. Rep. No. 52*, Geneva, Switzerland.
World Meteorological Organization (WMO) (2014), Scientific assessment of ozone depletion: 2014. *Glob. Ozone Res. and Monit. Proj. Rep. No. 55*, Geneva, Switzerland.